The CLEC-2–podoplanin axis controls fibroblastic reticular cell contractility and lymph node microarchitecture

Published in final edited form as:
Nat Immunol. 2015 January ; 16(1): 75–84. doi:10.1038/ni.3035.

The CLEC-2–podoplanin axis controls fibroblastic reticular cell contractility and lymph node microarchitecture

Jillian L. Astarita[1,2], **Viviana Cremasco**[2], **Jianxin Fu**[3,4], **Max C. Darnell**[5,6], **James R. Peck**[2], **Janice M. Nieves-Bonilla**[2], **Kai Song**[3,4], **Matthew C. Woodruff**[1,7], **Alvin Gogineni**[8], **Lucas Onder**[9], **Burkhard Ludewig**[9], **Robby M. Weimer**[8], **Michael C. Carroll**[7], **David J. Mooney**[5,6], **Lijun Xia**[3,4], and **Shannon J. Turley**[2,10,11]

[1]Division of Medical Sciences, Harvard Medical School, Boston, MA 02115, USA [2]Department of Cancer Immunology and AIDS, Dana Farber Cancer Institute, Boston, Massachusetts, 02115 [3]Cardiovascular Biology Research Program, Oklahoma Medical Research Foundation, Oklahoma City, Oklahoma 73104, USA [4]Department of Biochemistry and Molecular Biology, University of Oklahoma Health Sciences Center, Oklahoma City, Oklahoma 73104, USA [5]School of Engineering and Applied Sciences, Harvard University, Cambridge, MA 02138, USA [6]Wyss Institute for Biologically-Inspired Engineering at Harvard University, Cambridge, MA 02138, USA [7]Program in Cellular and Molecular Medicine, Children's Hospital Boston, Harvard Medical School, Boston, MA 02115, USA [8]Department of Biomedical Imaging, Genentech, South San Francisco, California, United States of America [9]Institute of Immunobiology, Kantonal Hospital St. Gallen, 9007 St. Gallen, Switzerland [10]Department of Microbiology and Immunobiology, Harvard Medical School, Boston, MA 02115, USA [11]Department of Cancer Immunology, Genentech, 1 DNA Way, South San Francisco, California, 94080

Abstract

In lymph nodes, fibroblastic reticular cells (FRCs) form a collagen-based reticular network that supports migratory dendritic cells (DCs) and T cells and transports lymph. A hallmark of FRCs is their propensity to contract collagen, yet this function is poorly understood. Here, we demonstrate that podoplanin (PDPN) regulated actomyosin contractility in FRCs. Under resting conditions, when FRCs are unlikely to encounter mature DCs expressing the PDPN receptor, CLEC-2, PDPN endowed FRCs with contractile function and exerted tension within the reticulum. Upon inflammation, CLEC-2 on mature DCs potently attenuated PDPN-mediated contractility, resulting in FRC relaxation and reduced tissue stiffness. Disrupting PDPN function altered the homeostasis and spacing of FRCs and T cells, resulting in an expanded reticular network and enhanced immunity.

Correspondence should be addressed to S.J.T. (turley.shannon@gene.com), Shannon J. Turley, Ph.D., Tel: 650-225-2790, Fax: 650-742-1580.

Author contributions

J.L.A and S.J.T. designed experiments, analyzed results, and wrote the manuscript. J.F., K.S., and L.X. supplied key reagents and mice. J.L.A., V.C., J.F., M.C.D, J.R.P., J.M.N-B., A.G., R.M.W., and M.C.W. performed experiments. L.O. and B.L. provided mice. L.X., D.J.M., V.C., M.C.C., and B.L. provided comments on the manuscript.

Competing financial interests

A.G. and R.M.W. are employees of Genentech.

Lymph nodes (LNs) are highly organized structures that serve as rendezvous points for dendritic cells (DCs) and T and B lymphocytes. The maintenance of LN structure and compartmentalization are critical for generating effective immune responses and controlling unwanted immune activation[1]. LNs increase vastly in size during immune responses and then must contract again upon resolution. Although lymphocyte proliferation and vascular remodeling contribute to this swelling[2–4], the contributions of the reticular network have not been elucidated.

Fibroblastic reticular cells (FRCs) are LN-resident mesenchymal cells that secrete and remodel extracellular matrix (ECM) to create a dense reticular network. The FRC network serves as a scaffold for DCs and T cells to crawl on[5–9] and as a conduit for transporting lymph from the subcapsular sinus into the LN parenchyma[7,10,11]. A propensity to pull on collagen fibers and create tension is a hallmark of myofibroblasts. FRCs are specialized myofibroblasts in lymphoid organs with notable contractility[7,8], however, the mechanistic basis and functional impacts of this hallmark remain unknown. We hypothesized that the contractile function of FRCs may play a role in tuning LN microarchitecture and immunity.

Podoplanin (PDPN; also known as gp38, Aggrus, and T1α) is a transmembrane glycoprotein highly expressed by FRCs, lymphatic endothelial cells (LECs), and multiple other cell types outside LNs[12]. It is critical during fetal development for blood-lymph separation and lung organogenesis[12–14], and its overexpression in cancer correlates with increased invasion and metastasis[15]. However, a cell-autonomous function of PDPN in healthy adults has yet to be elucidated. PDPN is the endogenous ligand for the C-type lectin receptor, CLEC-2 (also known as CLEC1b)[16], which is expressed by platelets and DCs. CLEC-2 signaling is critical for platelet activation[17], migration of activated DCs to draining LNs[18], and maintenance of vascular integrity and LN structure[19–21]. However, whether CLEC-2 engagement of PDPN results in signaling into the PDPN-expressing cell is unknown.

Here, we elucidate the role of the PDPN–CLEC-2 interaction in FRC function. Under resting conditions, when FRCs are unlikely to encounter CLEC-2 in LNs due to a dearth of migratory DCs[22], PDPN endows FRCs with a remarkable capacity to exert tension within the reticular network. In this state, PDPN activates the actomyosin machinery of FRCs by engaging a neighboring transmembrane protein. Preventing PDPN signaling by the provision of CLEC-2, antibody blockade, or genetic deficiency markedly attenuated myosin light chain (MLC) phosphorylation and FRC contraction. Loss of FRC contractility led to significant changes in the homeostasis and spacing of FRCs and T cells, with profound consequences for the LN microarchitecture and the expansion of antigen-specific T cells following immunization.

In sum, our results identify PDPN as a master regulator of actomyosin contractility in FRCs. PDPN signaling maintains FRCs in a highly contracted state in healthy, resting organs. Upon an inflammatory response, the interaction between migratory DCs and FRCs allowed CLEC-2 to block PDPN, thereby attenuating contractility and relaxing the reticulum. Consequently, these microanatomical changes allowed the LN to increase in size and meet the spatial demands of the expanding lymphocyte pool.

Results

PDPN regulates FRC actomyosin contractility

To investigate the function of PDPN in LN FRCs, we initially isolated FRCs from wild-type or *Pdpn*$^{-/-}$ mice. While *Pdpn*$^{-/-}$ mice generally die soon after birth due to blood-lymph mixing and edema, when crossed onto a C57BL/6 background, approximately 20% of mice thrive and served as a source of *Pdpn*$^{-/-}$ FRCs for our study[14]. FRCs from *Pdpn*$^{-/-}$ mice expressed normal amounts of canonical FRC markers including PDGFRα, PDGFRβ, CD44, α-smooth muscle actin, and cadherin 11 (Supplementary Fig. 1a). We first examined whether *Pdpn*$^{-/-}$ FRCs were defective in adhering to and spreading on collagen, as the converse has been reported for cancer cells overexpressing PDPN[23]. Indeed, *Pdpn*$^{-/-}$ FRCs were significantly impaired in both processes (Supplementary Fig. 1b,c). Next we sought to investigate the impact of PDPN deficiency on the FRC cytoskeleton in collagen-based three-dimensional (3D) deformable matrices, which more closely simulate the LN microenvironment[18]. PDPN-deficient FRCs were elongated and extended f-actin-rich membrane protrusions (Fig. 1a,b). Such protrusions were less abundant on *Pdpn*$^{-/-}$ FRCs; however, each protrusion extending from the cell body of *Pdpn*$^{-/-}$ FRCs was markedly longer than those of wild-type FRCs (Fig. 1c,d). Finally, as in 2D, PDPN-deficient FRCs covered a smaller area in 3D compared with wild-type FRCs (Fig. 1e).

Given that adhesion and spreading are related to cell contraction, we next examined whether PDPN influences FRC contractility utilizing multiple approaches. First, FRCs were treated with Y27632, an inhibitor of Rho-associated protein kinase (ROCK), a master regulator of contractility[24]. Y27632-treated FRCs exhibited extensive cell elongation similar to *Pdpn*$^{-/-}$ FRCs; however, Y27632-treated FRCs exhibited more protrusions than *Pdpn*$^{-/-}$ FRCs, suggesting that PDPN may signal through additional pathways (Supplementary Fig. 1d – f). Next, we directly assessed contractility by examining 3D collagen gel contraction. Wild-type FRCs were markedly more efficient at contracting collagen than *Pdpn*$^{-/-}$ FRCs (Fig. 1f). Finally, as a third measure of contractility, we examined the abundance of nuclear (active) yes-associated protein (YAP), a transcription factor recently reported to control contractility and promote the tumor-supporting functions of cancer-associated fibroblasts[25]. In agreement with the collagen contraction data, *Pdpn*$^{-/-}$ FRCs exhibited significantly less nuclear YAP compared with wild-type FRCs (Fig. 1g and Supplementary Fig. 1g). Taken together, these results indicate that PDPN is a critical regulator of adhesion, elongation, and contraction in FRCs.

Molecular regulation of PDPN-mediated contractility

Next we sought to examine the mechanism underlying PDPN functions in FRCs. The only known proximal signaling mechanism by which PDPN exerts direct effects on the cytoskeleton is by binding to and activating ezrin, radixin, and moesin (ERM) family proteins through a cluster of basic residues in the cytoplasmic tail of PDPN[23,26]. To ascertain whether PDPN-mediated control of actomyosin contractility is mediated via this ERM binding site in primary FRCs, we generated knock-in mice in which PDPN lacking its cytoplasmic tail globally replaced full-length PDPN (hereafter referred to as Δcyto) (Supplementary Fig. 2a,b). These mice were viable and did not exhibit any gross

abnormalities. FRCs from LNs of Δcyto mice expressed normal amounts of PDPN, which did not become glycosylphosphatidylinositol-anchored (Supplementary Fig. 2c – f). Upon culturing Δcyto FRCs in 3D, we found that deletion of the 9 amino acid cytoplasmic tail was sufficient to recapitulate the elongated phenotype observed in the *Pdpn*$^{-/-}$ FRCs with fewer, longer membrane protrusions compared with wild-type FRCs (Fig. 2a – d). Unexpectedly, Δcyto FRCs were essentially identical to wild-type FRCs with respect to contractility, showing no impairment in collagen contraction or difference in the amount of active YAP (Fig. 2e,f and Supplementary Fig. 2g).

Given that direct binding of the PDPN cytoplasmic tail cytoskeleton linker proteins appeared to be dispensable for actomyosin contractility in FRCs, we sought to examine whether and to what extent key mediators of actomyosin contractility were affected by PDPN deficiency. Whereas localization of phosphorylated ezrin was unchanged (Fig. 3a), phosphorylated (p)-ERM abundance was reduced by 50% in *Pdpn*$^{-/-}$ FRCs compared with wild-type and Δcyto FRCs (Fig. 3b and Supplementary Fig. 3a). The degree to which p-ERM abundance was reduced in *Pdpn*$^{-/-}$ FRCs was especially striking given that cytoskeletal linkers associate with multiple abundantly expressed transmembrane proteins. This idea, together with the finding that p-ERM abundance was normal in Δcyto FRCs, indicates that other domains of PDPN are sufficient to maintain global ERM activation.

Next, the subcellular localization of phosphorylated myosin light chain (p-MLC), a key regulator of contractility, was examined. In wild-type and Δcyto FRCs, p-MLC largely co-localized with actin filaments (Fig. 3c). In contrast, and consistent with the functional contraction data, in *Pdpn*$^{-/-}$ FRCs, the p-MLC molecules were not associated with actin filaments; instead, they were more evenly distributed throughout the cell (Fig. 3c). This finding was confirmed by immunoblot, which indicated that pMLC amounts were diminished in *Pdpn*$^{-/-}$ FRCs but comparable between wild-type and Δcyto FRCs (Fig. 3d and Supplementary Fig. 3b).

Finally, the abundance of active RhoA was measured in FRCs. This small GTPase is downstream of ERM signaling, but can also feedback to affect ERM activation[27]. Additionally, RhoA functions upstream of MLC to control contraction[24]. Consistent with our contraction data, RhoA-GTP was decreased in *Pdpn*$^{-/-}$ FRCs compared with wild-type and Δcyto FRCs, which had comparable amounts (Fig. 3e and Supplementary Fig. 3c). Together, these results indicate that PDPN expression maintains high amounts of activated ERM, MLC, and RhoA, which endow FRCs with contractile ability. When PDPN is genetically ablated, the global abundance of these activated factors are severely reduced and thus FRCs can no longer adhere to collagen and generate tension within the reticular network.

PDPN controls FRC proliferation and survival

Stromal fibroblasts are exquisitely sensitive to the stiffness of the ECM they adhere to, which in turn affects their cytoskeletal contraction. Elevated substrate stiffness incites tension in fibroblasts, which can affect their growth and survival[28]. Thus, we examined whether the attenuated contractility in *Pdpn*$^{-/-}$ FRCs affected their proliferation or survival. Whereas wild-type and Δcyto FRC numbers remained steady over a 4 day period, *Pdpn*$^{-/-}$

FRCs increased up to 4-fold in number (Fig. 4a). FRCs from *Pdpn*$^{-/-}$ mice proliferated more extensively than wild-type FRCs (Fig. 4b,c) and survived better than either wild-type or Δcyto FRCs (Fig. 4d,e). Overall, these data demonstrate that PDPN signaling is involved in regulating the growth and survival of FRCs.

PDPN controls LN stiffness and FRC proliferation

Given the effects of PDPN deficiency on the FRC cytoskeleton and actomyosin contractility on a cellular level, we next examined the effect of blocking PDPN on the FRC network *in vivo*. Due to the reduced viability of global *Pdpn*$^{-/-}$ mice, we utilized a PDPN blocking antibody (clone 8.1.1) that recapitulates both the elongation and impaired contraction observed in *Pdpn*$^{-/-}$ FRCs (Supplementary Fig. 4a,b). We administered 8.1.1 i.v. into wild-type mice or *Ccl19*-Cre^{+}*Rosa26*-eYFP$^{fl/fl}$ mice (in which eYFP expression is restricted to FRCs[29]) and examined LNs by flow cytometry and fluorescence microscopy. No gross abnormalities were observed, such as the bleeding reported in some transgenic mice[19,21], inflammation, or major disorganization of lymphocytes (Supplementary Fig. 4c – g and data not shown). However, skin-draining LNs were significantly enlarged and while there was a slight increase in cellularity, this increase was not concomitant with the increase in mass (Fig. 5a,b). This finding led us to question whether the stiffness of the LN was changed. Using a standard compression test we found that LNs were significantly less stiff and more deformable following PDPN blockade compared with isotype-treated controls (Fig. 5c).

Next, we asked whether FRCs would respond to this relaxation by increasing in number as they did *in vitro*. Two days after 8.1.1 administration, the number of BrdU^{+} (proliferating) FRCs and, accordingly, total FRC numbers, were significantly increased compared with isotype-treated mice (Fig. 5d,e). Additionally, FRCs in anti-PDPN-treated mice were significantly larger, consistent with a blasting phenotype (Supplementary Fig. 4h,i).

We also examined the impact of PDPN deficiency on FRCs using *Pdpn*$^{fl/fl}$*Pdgf*β-Cre^{+} mice in which FRCs lack PDPN[19]. Consistent with anti-PDPN-treated mice, *Pdpn*$^{fl/fl}$*Pdgf*β-Cre^{+} mice exhibited enlarged LNs with increased total cellularity and FRC numbers compared with *Pdpn*$^{fl/fl}$ controls (Supplementary Fig. 5a – c). However, additional studies in *Pdgf*β-Cre^{+}*Pdpn*$^{fl/fl}$ mice were not pursued due to the HEV-related bleeding phenotype that was previously reported[19] (Supplementary Fig. 5d).

Finally, we observed no differences in LN mass, total cellularity or FRC numbers in Δcyto mice compared with wild-type mice (Fig. 5f – h). Additionally, bleeding around HEVs was not observed in Δcyto mice (Supplementary Fig. 5e). Given that FRCs cultured from these mice exhibited an elongation phenotype but normal contractility, these *in vivo* results indicate that FRC contractility is critical for maintaining normal LN size and FRC cell numbers.

The FRC network expands upon PDPN blockade

Next, we sought to define the role of PDPN in the LN FRC network. First, conduit function was examined by injecting fluorescein isothiocyanate (FITC) into the footpad of isotype- or anti-PDPN-treated mice and collecting the popliteal LNs 4 h later. No obvious abnormalities

were noted in tracer access to conduits in either the paracortex or cortical regions beneath the SCS in anti-PDPN-treated mice (Supplementary Fig. 5f).

Next we examined the impact of PDPN blockade on structure of the FRC network at higher resolution. Confocal microscopy combined with 3D reconstruction and isosurface rendering revealed that the network had a finer appearance with increased space between fibers. Quantitative analysis confirmed that FRCs and ER-TR7 covered less surface area in LNs from anti-PDPN-treated mice compared with control animals (Fig. 5i – k). Similar changes to the FRC network were observed in *Pdpn*$^{fl/fl}$*Pdgf*β-Cre^{+} mice (Supplementary Fig. 5g – i). Finally, and consistent with our observations that LN mass and FRC numbers remained unchanged upon deletion of the PDPN cytoplasmic tail, the network structure in Δcyto LNs was similar to that in wild-type LNs (Fig. 5l – n).

To determine whether FRCs were further apart from one another, a nuclei distance analysis was performed in which the distance to the closest neighboring FRC nucleus was measured. FRCs in LNs of isotype-treated mice were closer to one another than those in anti-PDPN-treated mice (Fig. 5o and Supplementary Fig. 5j,k). Thus, the stromal relaxation that occurs upon attenuation of PDPN-mediated contractility leads to LN enlargement and expansion of the FRC network.

PDPN-mediated contractility restrains T cell responses

We next addressed how blocking PDPN function and FRC contractility would affect an immune response. To this end, wild-type mice were treated with the PDPN-specific antibody 2 days before receiving CFSE-labeled OT-I CD8^{+} T cells and immunization with lipopolysaccharide (LPS) and ovalbumin (OVA). Importantly, the PDPN-specific antibody did not block CLEC-2-Fc binding to FRCs or affect DC numbers in steady state or inflammatory conditions (Supplementary Fig. 6a – c). We found a significant increase in OT-I T cell numbers in anti-PDPN-treated LNs 96 h after immunization with LPS and OVA (Fig. 6a). Divided OT-I T cells were more abundant in anti-PDPN-treated LNs compared with control-treated LNs (Fig. 6b). We previously reported that FRCs suppress T cell proliferation under inflammatory conditions through cell-cell contact[30–33]. Given that we observed greater spacing between FRCs upon PDPN blockade, we examined whether there was a change in the numbers of T cells touching FRCs in the antibody-treated mice. Indeed, fewer T cells were in contact with the FRC network upon PDPN blockade compared with control mice (Fig. 6c), which may contribute to the increased T cell response. Overall, these findings indicate that PDPN-mediated control of FRC contractility is critical for restraining LN swelling and T cell responses.

CLEC-2 engagement of PDPN inhibits FRC contraction

PDPN^{+} FRCs will come into contact with CLEC-2 on migratory DCs and platelets[18,19,21], raising the question of how CLEC-2 binding to PDPN affects FRCs. To determine if CLEC-2 transmits a signal to FRCs, wild-type FRCs were cultured in 3D and incubated with soluble CLEC-2-Fc. Within 3 h, the FRCs became elongated, and by 12 h, they closely resembled *Pdpn*$^{-/-}$ FRCs (Fig. 7a,b). CLEC-2-Fc or control rabbit IgG had no effect on the elongation of *Pdpn*$^{-/-}$ or Δcyto FRCs (Supplementary Fig. 7a), as expected because FRCs

do not express Fc receptors[4]. In addition, treatment with CLEC-2-Fc impaired spreading of FRCs on collagen (Supplementary Fig. 7b). To determine whether the same effect could be achieved with CLEC-2 naturally expressed by cells, we co-cultured wild-type FRCs with LPS-activated wild-type or *Clec1b*$^{-/-}$ bone marrow-derived (BM) DCs or with wild-type or *Clec1b*$^{-/-}$ platelets. Notably, CLEC-2^{+} DCs and platelets induced elongation of FRCs to a similar degree as soluble CLEC-2-Fc (Fig. 7c,d). CLEC-2-Fc also induced PDPN clustering and formation of PDPN-rich protrusions (Fig. 7e,f). Thus, we examined whether this elongation was dependent on actin polymerization. Indeed, treatment with cytochalasin D at a concentration that preserved cytoskeletal integrity significantly reduced CLEC-2-Fc-elicited elongation in FRCs (Supplementary Fig. 7c).

That CLEC-2 had the same effect on FRCs as PDPN deficiency prompted us to test whether CLEC-2 binding inhibited contractility. As we observed in *Pdpn*$^{-/-}$ FRCs, CLEC-2 binding to wild-type and Δcyto FRCs caused a significant reduction in collagen contraction and nuclear-localized YAP (Fig. 7g–i and Supplementary Fig. 7d,e). These results are consistent with the extracellular domain of PDPN mediating contractility through lateral membrane interactions.

Finally, we tested whether CLEC-2 engagement of PDPN caused a decrease in active ERM and MLC similar to a deficiency in PDPN. Treatment of wild-type FRCs with CLEC-2-Fc caused a rapid and substantial decrease in both p-ERM and p-MLC (Fig. 7j,k and Supplementary Fig. 7f,g). Thus, the finding that CLEC-2 delivers a signal to FRCs recapitulating the effects of genetic PDPN deficiency suggests that CLEC-2 acts as an inhibitor of PDPN function.

CLEC-2 is required for LN expansion following immunization

Having shown that PDPN antibody blockade leads to increased LN swelling and T cell proliferation following immunization, and that CLEC-2 inhibits PDPN, we asked whether a CLEC-2 signal from DCs was necessary and sufficient to cause LN swelling. To this end, we injected wild-type and *Clec1b*$^{-/-}$ BMDCs into the footpads of wild-type mice and measured LN mass 1, 2, and 5 days later. We found that injection of wild-type BMDCs significantly increased LN mass as previously described[33], but injection of *Clec1b*$^{-/-}$ BMDCs led to significantly reduced swelling at each time point examined (Fig. 8a). While we previously published that *Clec1b*$^{-/-}$ BMDCs exhibit impaired migration to draining LNs, their numbers match those of wild-type BMDCs by day 3 (ref.[18]). Thus, the fact that LN mass was still significantly lower in animals that received *Clec1b*$^{-/-}$ BMDCs on day 5 supports our hypothesis that an inhibitory signal from CLEC-2 on migratory DCs is required for LN expansion.

Next, we hypothesized that a lack of CLEC-2 during an immune response would prevent the expansion of LNs and T cell proliferation. Thus, to examine the necessity of CLEC-2 on endogenous DCs, we immunized *Clec1b*$^{fl/fl}$ and *Clec1b*$^{fl/fl}$*Cd11c*-Cre^{+} mice with LPS and collected their LNs 24 h later. In agreement with our published data[18,34], we observed a dampened immune response, with smaller LNs and decreased total cellularity in *Clec1b*$^{fl/fl}$*Cd11c*-Cre^{+} compared with *Clec1b*$^{fl/fl}$ mice (Fig. 8b,c). As expected, this

observation was due to decreased numbers of migratory DCs entering the LN and a dampened T cell response (Fig. 8d,e).

Next, we asked whether a lack of CLEC-2 would impair expansion of the FRC network. While FRC numbers increased following immunization, this increase was dampened when the CLEC-2 signal from DCs was absent (Fig. 8f). Furthermore, as we observed in anti-PDPN-treated mice, the FRC network significantly expanded in *Clec1b*$^{fl/fl}$ control mice upon immunization (Fig. 8g – i, compare with Fig 5i). Interestingly, while there was no significant difference in the FRC network between control mice and *Clec1b*$^{fl/fl}$*Cd11c*-Cre^{+} mice in PBS-treated animals, the LPS-induced expansion of the network was abolished in *Clec1b*$^{fl/fl}$*Cd11c*-Cre^{+} mice (Fig. 8g – i). These results confirm our previously published findings that a lack of CLEC-2 impairs DC arrival in draining LNs and dampens immune responses. Furthermore, we advance those findings by demonstrating that the FRC network expands to accommodate increasing LN size and this expansion requires a CLEC-2 signal from DCs. While in this setting the effect CLEC-2 deficiency cannot be separated from that of impaired DC migration, these results nevertheless support our findings with the PDPN-specific antibody.

As a final test of whether CLEC-2 itself delivers a signal to relax the FRC network, we injected CLEC-2-Fc i.v. into wild-type mice and examined LNs at 1 and 4 h post-injection. Consistent with our hypothesis, after just 1 h, LNs were significantly larger than isotype-treated mice and, at 4 h, LNs had already returned nearly to baseline weight (Fig. 8j). This finding was not due to an influx of cells or inflammation (Supplementary Fig. 7h – l). LECs also express PDPN, raising the possibility that the CLEC-2 signal may alter vascular integrity. However, while *Pdpn*$^{-/-}$ LECs are elongated compared with wild-type LECs, unlike FRCs, wild-type LECs do not respond to soluble CLEC-2 by elongating (Supplementary Fig. 7m). Furthermore, injection of anti-PDPN did not lead to changes in lymphatic pulsatile activity at early (1 h) or late (48 h) time points (data not shown), suggesting that the *in vivo* effects of PDPN blockade are not attributable to alterations in lymph flow. However, in CLEC-2-Fc-treated LNs, FRCs were disorganized, particularly around HEVs. Thus, a relaxation of FRCs may alter HEV integrity and allow blood or plasma to enter LNs (Supplementary Fig. 7n).

Collectively, these data indicate that CLEC-2 signals FRCs to relax. This relaxation leads to increased spacing in the paracortical reticular network and allows LNs to expand. However, upon attenuation of the CLEC-2 signal, FRCs regain their contractile ability, restoring LN size and microarchitecture (Supplementary Fig. 8).

Discussion

Here, we identify PDPN as a master regulator of contractile force generated by FRCs and illuminate a critical function for FRC contractility in maintaining LN microarchitecture. Under non-inflammatory conditions, PDPN maintains FRCs in a highly contracted state. Disruption of PDPN-mediated contractility causes LN enlargement in part via relaxation and expansion of the FRC network. Notably, these changes did not affect conduit permeability,

in line with our recent report demonstrating prolonged conduit function following FRC ablation[35].

Importantly, we discovered that CLEC-2 inhibits PDPN signaling in FRCs. Previous studies of the PDPN-CLEC-2 interaction focused on signaling downstream of CLEC-2[18,19,21]. Here, we demonstrate that signaling also occurs downstream of PDPN and that its engagement by CLEC-2 on DCs diminishes FRC contractility. CLEC-2 appears to deliver a rapid and transient inhibitory signal to FRCs. The affinity of CLEC-2 binding PDPN is 24.5 μM[16], whereas a high affinity antibody can be in the nanomolar or even picomolar range[36]. Furthermore, within minutes of engaging soluble PDPN, CLEC-2 is internalized[18]. Thus, the inhibition of PDPN caused by migratory DCs would likely be quickly relieved.

Our finding that the cytoplasmic tail of PDPN is dispensable for FRC contractility was unexpected and suggests that its extracellular or transmembrane domains mediate this hallmark function. Indeed, the interaction of PDPN with CD44 and galectin-8 regulates cell migration and adhesion[37,38]. Furthermore PDPN interacts with CD9, which may play a role in regulating integrin function[39]. Furthermore, the transmembrane domain is required for PDPN localization to lipid rafts[40], where CD44 is also retained upon TGF-β-mediated differentiation of fibroblasts into myofibroblasts[41]. Additionally, our results indicating that the cytoplasmic tail was required for elongation despite displaying normal levels of activated ERMs indicates that the cytoplasmic tail has other signaling mechanisms. In fact, two serines within the tail can be phosphorylated[42]. To what extent these interactions regulate FRC function in the LN and organ microarchitecture remains unclear. That CLEC-2 inhibits contraction to the same extent in Δcyto and wild-type FRCs suggests that CLEC-2 mediates its effect by preventing the extracellular domain of PDPN from interacting in cis with a lateral binding partner.

Similar to FRCs, PDPN controls elongation and RhoA activation in LECs[43]; however, LECs differed from FRCs in that LECs did not elongate upon CLEC-2 binding. Furthermore, we found that bulk lymph flow and lymph access to conduits were not altered upon in vivo PDPN blockade. Given our results and that LECs are not highly contractile it is unlikely that LEC-expressed PDPN plays a role in LN expansion and reticular architecture.

Cell contractility and sensing of matrix stiffness regulate fibroblast differentiation, migration, and survival[44]. The balance between cell adhesion to a substrate of a given stiffness and the resulting tension within that cell determines overall tensional homeostasis[44,45]. Disruption of this balance, whether by changes in matrix stiffness or contractile potential, alters fibroblast proliferation[46]. Thus, the increased proliferation and survival that we observed in *Pdpn*$^{-/-}$ FRCs may stem from dysregulated adhesion or tension or both.

Inflammation is known to trigger FRC proliferation; however, the timing and extent of division appears to vary between inflammatory stimuli, and the specific underlying mechanisms remain unknown[4,34,47]. Our data indicate that the relaxation of FRCs allows for early LN expansion in addition to providing a signal for proliferation, which causes FRCs to accumulate and accommodate the expanding organ. While a previous study[47] did not report

changes in LN architecture, we (here and ref. 34) observed an expansion in the FRC network upon immunization. This discrepancy could be due to differences in the timing or types of immunization used. Intriguingly, it was noted here and elsewhere ([47,48] and data not shown) that PDPN amounts increase in response to select inflammatory stimuli, which may restore high contractility to FRCs upon resolution of inflammation. Our results demonstrate that this process is crucial for FRC-mediated restraint of T cell proliferation.

Together, these data indicate that CLEC-2$^+$ DCs provide a fast but reversible signal to PDPN$^+$ FRCs. This allows for a transient relaxation of the FRC network that would persist only as long as CLEC-2$^+$ DCs were crawling along the network. Ultimately, normal contraction of FRCs would resume shortly after the removal of the CLEC-2 signal (and increased PDPN expression), which would occur as the immune response begins to wane and migratory DCs perish in the draining LN. Re-establishment of FRC contractility would enable structural and functional homeostasis in the reticular network to be restored.

Online Methods

Mice

C57BL/6 mice were purchased from Jackson Laboratory (strain 000664). *Ccl19*-Cre mice were generated as previously described[29] and were crossed to *Rosa26*-eYFP mice (Jackson Laboratory, strain 006148) to generate mice where only FRCs express eYFP. The *Ccl19*-Cre mice were also mated to B6;129-*Gt-Rosa26Sor*^{tm1Ytchn}/*J* (Jackson Laboratory stain 021847) for the nuclei distance analysis experiments. The *Pdgfr*β-Cre and *Pdpn*-flox mice were generated and initially characterized previously[19].

To determine the cytoplasmic function of PDPN, we generated knock-in mice lacking the cytoplasmic tail of PDPN (Δcyto). To delete the cytoplasmic domain, we made a targeting construct that introduced three stop codons immediately after the sequence encoding its transmembrane domain. C57BL/6 embryonic stem (ES) cells were used for gene targeting. A neomycin cassette flanked by Frt sites was used for selection of positive ES clones. Diptheria toxin A was used for negative selection. Two positive ES clones were injected into C57BL/6J blastocytes, which were then implanted into pseudopregnant mice. Chimeras among the offspring were bred with C57BL/6J FLP mice (B6.Cg-Tg (ACTFLEe)9205Dym/J, Jackson Laboratories) to test germline transmission and to delete the Frt flanked neomycin cassette. Genotypes of mice were determined by conducting PCR on DNA isolated from tail biopsies. Four chimeras transmitted the PDPN knock-in mutation into their offspring. Breeding with the FLP mice also successfully deleted the Frt flanked neomycin cassette in the F1 generation.

Mice were maintained under specific pathogen-free conditions as mandated by the National Institutes of Health guidelines. The mice were used between 4–7 weeks of age and were age- and sex-matched for all experiments. Animal studies were approved by the Research Animal Care committees of Dana-Farber Cancer Institute and Genentech.

Stromal cell isolation

For cell culture or flow cytometric analysis, stromal cells were isolated from LNs as previously described[49]. Briefly, skin-draining and mesenteric LNs were incubated in digestion media (RPMI containing 0.1 mg/ml DNase I (Invitrogen), 0.2 mg/ml Collagenase P (Roche) and 0.8 mg/ml Dispase (Roche)) and cell fractions were collected every 10–15 m over a period of 45 m. The single cell suspension was filtered and either plated in α-MEM containing 10% FBS and 1% penicillin-streptomycin or were stained with antibodies for flow cytometric analysis.

FRC purification

After LN digestion and plating, the non-adherent hematopoietic cells were washed away and the remaining stromal cells were allowed to grow for 5–7 days. To purify FRCs from this mixed culture, cells were trypsinized and incubated with biotinylated CD31- and CD45-specific antibodies (clones MEC13.3 and 30-F11, respectively) for 10 m. After washing, the cells were incubated with α-biotin microbeads for 15 m. Then the cells were washed, run through an LS magnetic-activated cell-sorting column (Miltenyi Biotech), and the flow-through containing FRCs was collected. FRCs used in experiments were greater than 85% pure.

3D Matrigel cultures and imaging

For 3D cultures, gels were prepared as previously described[18]. Briefly, 1.5×10^4 FRCs were mixed with 100 μL of the Matrigel mix (1.8 mg/ml reduced growth factor Matrigel (BD Biosciences) and 3.2 mg/ml type I collagen (BD biosciences)) and plated in glass-bottom 24-well plates (MatTek Corporation). For treatment conditions, a final concentration of 10 μg/mL anti-PDPN (Biolegend, clone 8.1.1), 7 μg/mL CLEC-2-Fc (made in-house[18]), or appropriate controls were added to the cell suspensions 15 m before the addition of the Matrigel mix. For short-term treatments, the cells were allowed to populate the gels for 24 h and then 250 nm cytochalasin D (Sigma), 10 μm Y27632 (Sigma), or 7 μg/mL CLEC-2-Fc were added directly to the media. To image the cells, the media was removed and the gels were washed twice in PBS. Next, cells were fixed in 4% paraformaldehyde (PFA; Affymetrix), washed, and permeabilized in 0.25% Triton-X. Cells were then stained with DAPI and rhodamine phalloidin (Invitrogen). The gels were washed with PBS and imaged with a Leica SP5X laser-scanning confocal microscope. *z*-stack projections were generated in ImageJ (imagej.nih.gov), and the area and perimeter of the cells were measured. The morphology index was calculated with the following equation: $\text{perimeter}^2/4*\pi*\text{area}$.

FRC spreading and adhesion

For spreading, 10 cm dishes were coated with type I collagen according to the manufacturer's instructions (BD Biosciences). FRCs were plated and imaged with a light microscope at the indicated times. Cell area was determined with ImageJ. For adhesion, 96-well plates were coated with collagen and 2×10^3 FRCs per well were added. At the indicated times, the wells were washed 3 times with PBS to remove non-adherent cells and the adherent cells were fixed in 4% PFA then stained with crystal violet. After several

washes to remove unbound crystal violet, the cells were lysed in 0.25% Triton-X and the absorbance of crystal violet was determined with a spectrophotometer at 570 nm.

Immunoblotting

Purified FRCs were plated in 10 cm dishes at a density of 3×10^5 cells per plate overnight. Cells were serum-starved for 5 h and then were lysed in lysis buffer (25 mM Tris-HCl pH 7.4, 150 mM NaCl, 1 mM EDTA, 1% NP-40 and 5% glycerol; Thermo Scientific) containing protease and phosphatase inhibitor cocktails (Thermo Scientific). Protein concentration was determined with the BCA protein assay kit (Thermo Scientific). Equal amounts of protein were loaded onto 4–12% Bis-Tris gels (Life Technologies) and then transferred to a nitrocellulose membrane. After blocking in 5% non-fat milk for 1 h, the membranes were incubated with primary antibodies in 5% BSA overnight. The following primary antibodies were used: anti-ERM (#3142), anti-p-ERM (#3149), anti-MLC (#8505), and anti-p-MLC (S19, #3671) (all from Cell Signaling Technology). After 3 washes with TBS, the membranes were incubated with anti-rabbit-IgG conjugated to HRP (Cell Signaling Technology) for two h at 25 °C. Finally, the signal was visualized with the SuperSignal WestDura Chemiluminescent Substrate (Fisher).

GTPase pulldowns

For each condition, 7.5×10^5 wild-type, *Pdpn*$^{-/-}$, and Δ*cyto* FRCs were plated in 10 cm dishes, and the activation of RhoA were determined with an active RhoA pulldown kit (Thermo Scientific), following the manufacturer's instructions. Immunoblots were performed with anti-RhoA (Thermo Scientific) followed by an anti-rabbit-HRP secondary (Cell Signaling).

Gel contraction assay

For contraction assays, 1.0×10^4 cells were mixed with 50.μL of the Matrigel mix and plated in 96-well culture dishes. Once the gels polymerized, 100 μL of media was added to the wells, and gels were detached from wells of the plate with a sterile pipette tip. After 24 h, images were taken of the wells and dimensions of gels were measured relative to well diameter in ImageJ. Alternatively, cells were allowed to seed the gel overnight, then CLEC-2-Fc or the 8.1.1 antibody were added every 4–8 h and the contraction was measure 24 h later.

Proliferation assays

Wild-type, *Pdpn*$^{-/-}$, and Δ*cyto* FRCs were plated in triplicate at a density of 2×10^3 cells per well in a 96-well plate and the number of viable cells was measured daily over the course of 4 days, using the CellTiter-Glo Luminescent Cell Viability Assay (Promega), according to the manufacturer's instructions. Data were normalized to the number of cells present on day 1 for each condition. To determine cell proliferation, 3.0×10^4 FRCs were labeled with 1 μM of Carboxyfluorescein succinimidyl ester (CFSE; Invitrogen) and plated in 6-well plates. On days 1, 2, 3, and 4, the cells were trypsinized and analyzed by flow cytometry to determine the mean fluorescent intensity of the CFSE dye.

YAP staining

Wild-type or *Pdpn*$^{-/-}$ FRCs were plated on eight well chamber slides and allowed to adhere for 12 h in order to minimize the role of differential cell spreading in the quantification of nuclear YAP. Where indicated, CLEC-2-Fc was added to the medium for 15 m prior to seeding. After 12 h, the media was changed and fresh medium either containing CLEC-2-Fc or not was added. At each time point, cells were fixed for 15 m with 4% PFA and washed 3 times for 5 m in PBS. Immunostaining was performed with rabbit anti-mouse YAP/TAZ (Cell Signaling #8418) and visualized with a goat anti-rabbit secondary conjugated to Alexa-555 (Cell Signaling) per the manufacturer's instructions. Nuclei were counterstained with DAPI. The percentage of nuclear YAP was quantified using MATLAB software by summing the fluorescence intensity within the region masked by the nucleus compared to the total fluorescence intensity on a per-cell basis.

In vivo PDPN blockade

Mice were injected i.v. into the tail vein with 100 μg of purified anti-PDPN (Biolegend clone 8.1.1) or the hamster IgG isotype control antibody (Biolegend clone SHG-1). After 48 or 96 h, mice were sacrificed and skin-draining LNs were collected for either flow cytometric analysis or imaging. For CLEC-2-Fc experiments, 100 μg of CLEC-2-Fc or rabbit IgG isotype control (R&D) was injected i.v. and LNs were collected 1 and 4 h later. Generally, flow cytometric analyses were conducted on brachial LNs and imaging was conducted with axillary and brachial LNs or inguinal LNs for immunization experiments.

Compression test

Mice were treated with the hamster isotype control or anti-PDPN 48 h prior to LN collection. Cylindrical discs (1.3 mm^2) were punched from LNs with a biopsy punch to ensure a consistent cross-sectional area. These samples were subjected to compression using an Instron mechanical tester at a strain rate of 0.5 mm/m, and the stiffness was calculated as the slope of the first 10% of the resulting stress/strain curve.

Nuclei distance analysis

Ccl19-Cre^{+} x *Rosa26Sor*^{tm1Ytchn}/*J*$^{fl/WT}$ mice were injected with 100 μg of anti-PDPN or isotype control i.v., and axillary and brachial LNs were collected 48 h later. LN sections were stained with anti-GFP (A10263 from Life Technologies) and an anti-rabbit secondary conjugated to Alexa488 (Molecular Probes). Images of the FRC nuclei were collected and analyzed with CellProfiler[50] using the neighbor analysis module.

T cell-FRC interactions ex vivo

To measure the numbers of T cells in contact with FRCs, isotype and PDPN-specific antibodies were injected i.v. into *Ccl19*-Cre^{+}*Rosa26*-eYFP mice. One day later, 5 × 10^6 purified T cells labeled with Far Red cell tracker (Invitrogen) were injected i.v. The mice were sacrificed 24 h later, and LNs were fixed and imaged. Imaris software was used to generate isosurfaces for the T cells and the FRC network, and the numbers of T cells in contact with the FRC network were determined.

Immunizations

To investigate the role of PDPN during an immune response, BoyJ mice were first given the 8.1.1 antibody as described above. Two days later, 1×10^6 CFSE-labeled CD45.2$^+$ OT-I T cells were injected i.v. into each mouse. 4 h later, mice received 500 μg of OVA and 30 μg of LPS i.v., and a second dose of the isotype control and PDPN-specific antibodies was administered 24 h later. Mice were analyzed 24 and 48 h after administration of the OT-I T cells, LPS, and OVA. Brachial LNs were collected and digested for flow cytometry analysis, while inguinal LNs were collected and fixed for imaging.

For immunizations in *Cd11c*-Cre x *Clec1b*-flox mice, PBS or 8 μg of LPS was injected s.c. in the hind and fore footpads. LNs were collected 24 h later for flow cytometry (popliteal) or imaging (axillary and brachial).

Flow cytometric analysis and antibodies

After the enzymatic LN digestion, cells were resuspended in flow cytometry buffer (PBS containing 2% FBS and 2 mM EDTA) and were incubated for 15 m with antibodies against the following surface markers: PDPN (clone 8.1.1, Biolegend), CD31 (clone MEC13.3, Biolegend), CD45 (clone 30-F11, Biolegend), B220 (clone RA3–6B2, eBioscience), CD3ε (clone 17A2, Biolegend), CD4 (clone RM 4–5, eBioscience), CD8 (clone 53-6.7, Biolegend). For the BrdU labeling, mice were injected i.p. with 2 mg of BrdU 24 h before analysis. Cells were stained with the BrdU flow kit according to the manufacturer's instructions (BD Pharmingen). Cells were then analyzed on either a FACSCalibur or a FACSAria (both from BD Biosciences). Flow cytometer data were analyzed with FlowJo.

Immunofluorescence staining of cells and tissue sections

Cells were plated on collagen-coated coverslips and allowed to adhere overnight. Then they were washed with PBS, fixed in 4% PFA for 10 m, and permeabilized with 0.25% Triton-X before staining with α-PDPN (clone 8.1.1, Biolegend). LNs were collected, fixed in 4% PFA for 4 h, and incubated in 30% sucrose in PBS overnight. LNs were frozen in optimal cutting temperature media (Fisher Scientific) on dry ice and then 20–80 μm sections were cut with a cryostat. Slides were stained immediately or stored at −80 °C. Sections were fixed in 4% PFA for 10 m, permeabilized with 0.25% Triton-X for 3 m, and then blocked with 2% BSA in PBS for 30 m before incubation with antibodies. The sections were incubated with were anti-ER-TR7 (AbCam #ab51824), anti-GFP (Molecular Probes), and anti-PNAd-biotin (clone MECA-79, Biolegend) for 1 h, then washed 3 times with 2% BSA. The secondary antibodies anti-rat-Alexa-555, anti-rabbit-Alexa-488 and streptavidin-647 (all from Invitrogen) were then added for 30 m. After a final wash step, the slides were imaged on either a Leica SP5X laser-scanning confocal microscope or a Zeiss 710 two-photon laser-scanning confocal microscope. Images were analyzed with ImageJ. The surface area analysis was conducted with Imaris software (Bitplane AG, Zurich, Switzerland). For each set of images acquired on the same day, the parameters for the surfaces module were set for the control samples and the same parameters were used to analyze all images acquired in the same imaging session.

Tracer injection and conduit imaging

Wild-type mice were injected i.v. with the isotype control or PDPN-specific antibody. Four to 8 h later, they were injected subcutaneously in the footpad with 10 μL saturated FITC solution (Sigma) in HBSS (~0.1 mg/mL). Popliteal LNs were collected 4 h post injection and fixed in 4% PFA. LNs were optically cleared as previously described[30], and mounted as whole organ explants for multi-photon microscopy. Cortical and paracortical regions were identified by collagen density and the presence or absence of CR1-specific antibody staining, which recognizes follicular dendritic cells (clone 8C12, made in-house) of which 3 μg was injected i.v. 6 h prior to the start of the experiment.

Isolation of platelets and BMDCs from fetal liver chimeric mice

Clec1b$^{-/-}$ fetal liver chimeric (FLC) mice were generated as previously described[18]. Briefly, fetuses from pregnant *Clec1b*$^{+/-}$ mice were collected between days E14.5–18.5, and 1×10^6 fetal liver cells were then injected retro-orbitally into lethally irradiated *B6.SJL-Ptprc*^{a}*Pep3*^{b}*/BoyJ* mice (Jackson Laboratories). Mice were used 6–7 weeks later for experiments. BMDCs were generated as previously described[18]. Briefly, bone marrow was collected from the tibias and femurs of the FLCs and cultured in RPMI containing 10% FBS and 3% GM-CSF for 5–7 days. For studies where BMDCs were injected, they were matured with 50 ng/mL LPS on day 7. Then 1.4×10^6 BMDCs were injected into the footpad and popliteal LNs were collected and weighed 1, 2, and 5 days later.

Platelets were isolated as previously described[20]. Briefly, approximately 500 μL whole blood was collected from the FLCs by retro-orbital bleeds into 3.8% sodium citrate. Red blood cells were lysed in ACK lysing buffer (Fisher). Then the cells were resuspended and centrifuged at 300*g* for 10 m with no break. The supernatant was collected and centrifuged again at 1,000*g* to collect the platelet-rich fraction. BMDCs and platelets were seeded into 3D gels at a ratio of 5:1 to the FRCs.

Statistical analysis

Statistical analyses were conducted with Prism (GraphPad Software, Inc.). If data was not normally distributed or did not have equal variance between conditions, a Mann Whitney U test was performed. For normally-distributed data, a Student's *t*-test was used. In some cases, a one sample *t*-test was employed to calculate whether a sample was statistically different from 1. Data were considered statistically significant when $P < 0.05$. In cases where multiple statistical tests were performed, a Bonferroni correction was used to determine a new alpha cut-off for significance. Observers were not blinded to experimental conditions.

Supplementary Material

Refer to Web version on PubMed Central for supplementary material.

Acknowledgements

We would like to thank L. Cameron for her assistance at the Dana-Farber Cancer Institute confocal microscopy core. We are thankful for the help that Rebecca Gelman provided with statistical analyses. This work was supported

by grants from the National Institutes of Health (ROI DK074500, PO1 AI045757, and R21 CA182598 to S.J.T.; 5R01 AI039246 to M.C.C.; and P01 HL085607 to L.X.), an American Cancer Society Research Scholar Grant (to S.J.T.), a Claudia Adams Barr Award for Innovative Cancer Research (to S.J.T.), a Cancer Research Institute Fellowship (to V.C.), an American Heart Association grant (SDG7410022 to J.F.), and a National Science Foundation Graduate Research Fellowship (to J.L.A.).

References

1. Andrian, von UH, Mempel TR. Homing and cellular traffic in lymph nodes. Nat. Rev. Immunol. 2003; 3:867–878. [PubMed: 14668803]
2. Kumamoto Y, Mattei LM, Sellers S, Payne GW, Iwasaki A. CD4+ T cells support cytotoxic T lymphocyte priming by controlling lymph node input. P. Natl. Acad. Sci. USA. 2011; 108:8749–8754.
3. Tzeng TC, et al. CD11chi Dendritic Cells Regulate the Re-establishment of Vascular Quiescence and Stabilization after Immune Stimulation of Lymph Nodes. J. Immunol. 2010; 184:4247–4257. [PubMed: 20231692]
4. Chyou S, et al. Coordinated Regulation of Lymph Node Vascular-Stromal Growth First by CD11c+ Cells and Then by T and B Cells. J. Immunol. 2011; 187:5558–5567. [PubMed: 22031764]
5. Turley SJ, Fletcher AL, Elpek KG. The stromal and haematopoietic antigen-presenting cells that reside in secondary lymphoid organs. Nat. Rev. Immunol. 2010; 10:813–825. [PubMed: 21088682]
6. Malhotra D, Fletcher AL, Turley SJ. Stromal and hematopoietic cells in secondary lymphoid organs: partners in immunity. Immunol. Rev. 2013; 251:160–176. [PubMed: 23278748]
7. Malhotra D, et al. Transcriptional profiling of stroma from inflamed and resting lymph nodes defines immunological hallmarks. Nat. Immuno.l. 2012; 13:499–510.
8. Link A, et al. Fibroblastic reticular cells in lymph nodes regulate the homeostasis of naive T cells. Nat. Immunol. 2007; 8:1255–1265. [PubMed: 17893676]
9. Bajénoff M, et al. Stromal cell networks regulate lymphocyte entry, migration, and territoriality in lymph nodes. Immunity. 2006; 25:989–1001. [PubMed: 17112751]
10. Sixt M, et al. The conduit system transports soluble antigens from the afferent lymph to resident dendritic cells in the T cell area of the lymph node. Immunity. 2005; 22:19–29. [PubMed: 15664156]
11. Roozendaal R, Carroll MC. Complement receptors CD21 and CD35 in humoral immunity. Immunol. Rev. 2007; 219:157–166. [PubMed: 17850488]
12. Astarita JL, Acton SE, Turley SJ. Podoplanin: emerging functions in development, the immune system, and cancer. Front. Immunol. 2012; 3:283. [PubMed: 22988448]
13. Schacht V, et al. T1alpha/podoplanin deficiency disrupts normal lymphatic vasculature formation and causes lymphedema. EMBO. J. 2003; 22:3546–3556. [PubMed: 12853470]
14. Uhrin P, et al. Novel function for blood platelets and podoplanin in developmental separation of blood and lymphatic circulation. Blood. 2010; 115:3997–4005. [PubMed: 20110424]
15. Wicki A, Christofori G. The potential role of podoplanin in tumour invasion. Br. J. Cancer. 2006; 96:1–5. [PubMed: 17179989]
16. Christou CM, et al. Renal cells activate the platelet receptor CLEC-2 through podoplanin. Biochem. J. 2008; 411:133–140. [PubMed: 18215137]
17. Suzuki-Inoue K, Inoue O, Ozaki Y. Novel platelet activation receptor CLEC-2: from discovery to prospects. J. Thromb. Haemost. 2011; 9:44–55. [PubMed: 21781241]
18. Acton SE, et al. Podoplanin-rich stromal networks induce dendritic cell motility via activation of the C-type lectin receptor CLEC-2. Immunity. 2012; 37:276–289. [PubMed: 22884313]
19. Herzog BH, et al. Podoplanin maintains high endothelial venule integrity by interacting with platelet CLEC-2. Nature. 2014; 502:105–109. [PubMed: 23995678]
20. Hess PR, et al. Platelets mediate lymphovenous hemostasis to maintain blood-lymphatic separation throughout life. J. Clin. Invest. 2014; 124:273–284. [PubMed: 24292710]
21. Benezech C, et al. CLEC-2 is required for development and maintenance of lymph nodes. Blood. 2014; 123:3200–3207. [PubMed: 24532804]

22. Steinman RM, et al. Dendritic cell function in vivo during the steady state: a role in peripheral tolerance. Ann. NY. Acad. Sci. 2003; 987:15–25. [PubMed: 12727620]
23. Martin-Villar E, et al. Podoplanin binds ERM proteins to activate RhoA and promote epithelial-mesenchymal transition. J. Cell Sci. 2006; 119:4541–4553. [PubMed: 17046996]
24. Riento K, Ridley AJ. Rocks: multifunctional kinases in cell behaviour. Nat. Rev. Mol. Cell Biol. 2003; 4:446–456. [PubMed: 12778124]
25. Calvo F, et al. Mechanotransduction and YAP-dependent matrix remodelling is required for the generation and maintenance of cancer-associated fibroblasts. Nat. Cell Biol. 2013; 15:637–646. [PubMed: 23708000]
26. Wicki A, et al. Tumor invasion in the absence of epithelial-mesenchymal transition: Podoplanin-mediated remodeling of the actin cytoskeleton. Cancer Cell. 2006; 9:261–272. [PubMed: 16616332]
27. Fehon RG, McClatchey AI, Bretscher A. Organizing the cell cortex: the role of ERM proteins. Nat. Rev. Mol. Cell Biol. 2010:1–12. [PubMed: 20050302]
28. Larsen M, Artym VV, Green JA, Yamada KM. The matrix reorganized: extracellular matrix remodeling and integrin signaling. Curr. Opin. Cell Biol. 2006; 18:463–471. [PubMed: 16919434]
29. Chai Q, et al. Maturation of lymph node fibroblastic reticular cells from myofibroblastic precursors is critical for antiviral immunity. Immunity. 2013; 38:1013–1024. [PubMed: 23623380]
30. Lukacs-Kornek V, et al. Regulated release of nitric oxide by nonhematopoietic stroma controls expansion of the activated T cell pool in lymph nodes. Nat. Immunol. 2011; 12:1096–1104. [PubMed: 21926986]
31. Siegert S, et al. Fibroblastic reticular cells from lymph nodes attenuate T cell expansion by producing nitric oxide. PLoS ONE. 2011; 6:e27618. [PubMed: 22110693]
32. Khan O, et al. Regulation of T cell priming by lymphoid stroma. PLoS ONE. 2011; 6:e26138. [PubMed: 22110583]
33. Webster B, et al. Regulation of lymph node vascular growth by dendritic cells. J. Exp. Med. 2006; 203:1903–1913. [PubMed: 16831898]
34. Acton SE, et al. Dendritic cells control lymph node expansion via modulation of fibroblastic reticular network tension through CLEC-2/Podoplanin interactions. Nature. in press.
35. Cremasco V, et al. B cell homeostasis and follicle confines are governed by fibroblastic reticular cells. Nat. Immunol. 2014; 15:973–981. [PubMed: 25151489]
36. Andersson, K.; Björkelund, H.; Malmqvist, M. Antibody-antigen interactions: what is the required time to equilibrium?. 2010. Available from Nature Precedings <http://hdl.handle.net/10101/npre.2010.5218.1>
37. Martín-Villar E, et al. Podoplanin associates with CD44 to promote directional cell migration. Mol. Biol. Cell. 2010; 21:4387–4399. [PubMed: 20962267]
38. Cueni LN, Detmar M. Galectin-8 interacts with podoplanin and modulates lymphatic endothelial cell functions. Exp. Cell Res. 2009; 315:1715–1723. [PubMed: 19268462]
39. Nakazawa Y, et al. Tetraspanin family member CD9 inhibits Aggrus/podoplanin-induced platelet aggregation and suppresses pulmonary metastasis. Blood. 2008; 112:1730–1739. [PubMed: 18541721]
40. Fernández-Muñoz B, et al. The transmembrane domain of podoplanin is required for its association with lipid rafts and the induction of epithelial-mesenchymal transition. Int. J. Biochem. Cell B. 2011; 43:886–896.
41. Midgley AC, et al. Transforming growth factor-β1 (TGF-β1)-stimulated fibroblast to myofibroblast differentiation is mediated by hyaluronan (HA)-facilitated epidermal growth factor receptor (EGFR) and CD44 co-localization in lipid rafts. J. Biol. Chem. 2013; 288:14824–14838. [PubMed: 23589287]
42. Krishnan H, et al. Serines in the intracellular tail of podoplanin (PDPN) regulate cell motility. J. Biol. Chem. 2013; 288:12215–12221. [PubMed: 23530051]
43. Navarro A, Perez RE, Rezaiekhaligh M, Mabry SM, Ekekezie II. T1 /podoplanin is essential for capillary morphogenesis in lymphatic endothelial cells. Am. J. Physiol-Lung C. 2008; 295:L543–L551.

44. Paszek MJ, et al. Tensional homeostasis and the malignant phenotype. Cancer Cell. 2005; 8:241–254. [PubMed: 16169468]
45. Klein EA, et al. Cell-cycle control by physiological matrix elasticity and in vivo tissue stiffening. Curr. Biol. 2009; 19:1511–1518. [PubMed: 19765988]
46. Xia H, Nho RS, Kahm J, Kleidon J, Henke CA. Focal dhesion kinase Is upstream of phosphatidylinositol 3-kinase/Akt in regulating fibroblast survival in response to contraction of type I collagen matrices via a β1 integrin viability signaling pathway. J. Biol. Chem. 2004; 279:33024–33034. [PubMed: 15166238]
47. Yang CY, et al. Trapping of naive lymphocytes triggers rapid growth and remodeling of the fibroblast network in reactive murine lymph nodes. P. Natl. Acad. Sci. USA. 2014; 111:E109–E118.
48. Peduto L, et al. Inflammation recapitulates the ontogeny of lymphoid stromal cells. J. Immunol. 2009; 182:5789–5799. [PubMed: 19380827]
49. Fletcher AL, et al. Reproducible isolation of lymph node stromal cells reveals site-dependent differences in fibroblastic reticular cells. Front. Immunol. 2011; 2:35–50. [PubMed: 22566825]
50. Lamprecht M, Sabatini D, Carpenter A. CellProfiler™: free, versatile software for automated biological image analysis. Biotech. 2007; 42:71–75.

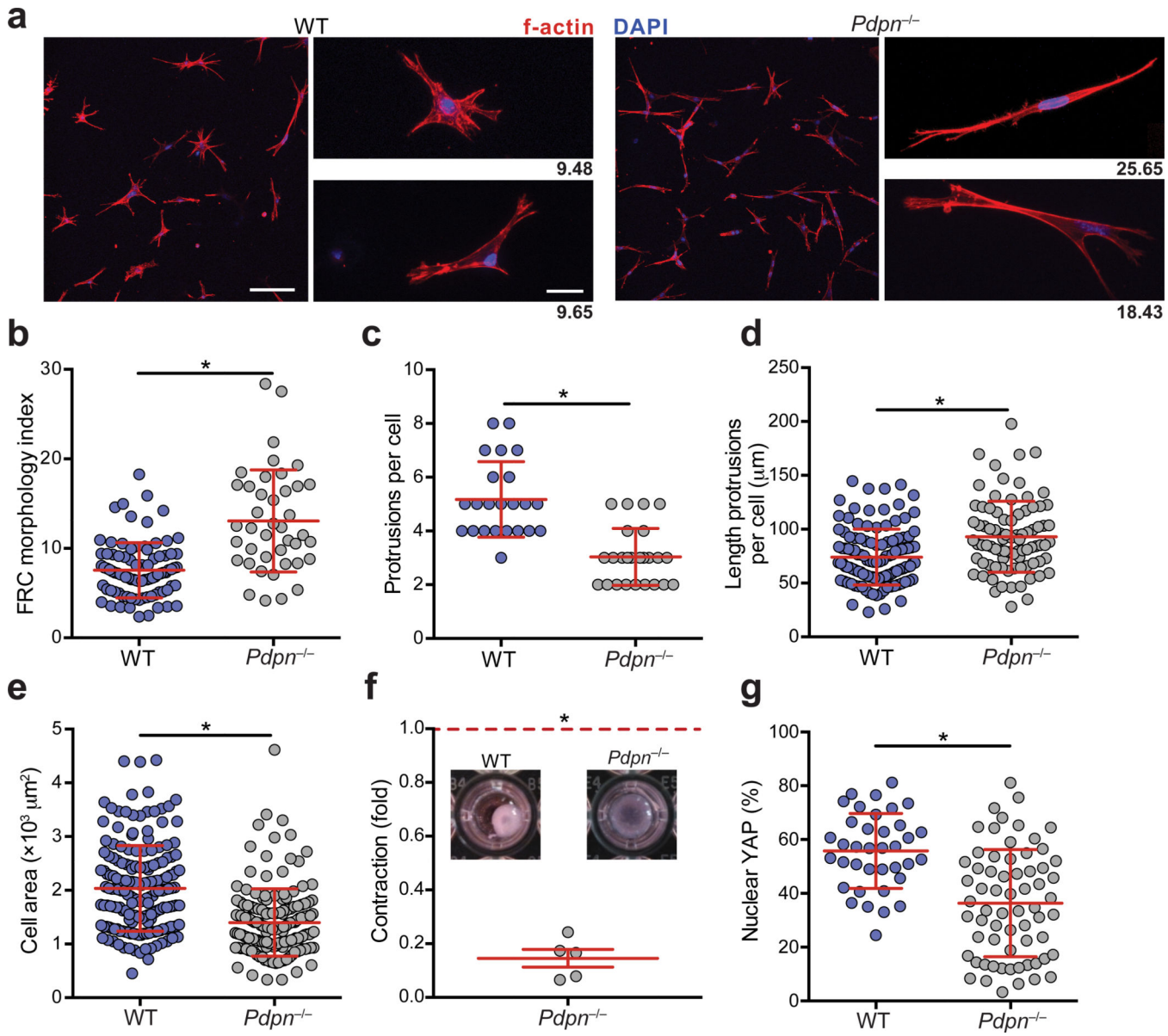

Figure 1. PDPN controls FRC spreading, elongation, and actomyosin contractility

(**a**) Confocal images of wild-type and *Pdpn*$^{-/-}$ FRCs seeded into 3D gels. Scale bar, 100 μm in low magnification images (left) and 20 μm in high magnification images (right). Numbers indicate the morphology index value for the cell pictured. (**b**) Quantification of FRC elongation (morphology index = perimeter^2/4πarea). (**c,d**) Graphs depict the number of protrusions per cell (**c**) and the lengths of individual protrusions (**d**) of FRCs. Data points represent cells from 3 independent experiments (mean±s.d., n>50 cells from 5 mice per experiment). (**e**) Quantification of the area covered by FRCs as they spread in collagen-based matrices. (**f**) Relative amount that *Pdpn*$^{-/-}$ FRCs contracted collagen gels relative to wild-type FRCs. Data representative 5 independent experiments (mean±s.d., 3 wells per experiment). (**g**) Percentages of nuclear-localized YAP in wild-type and *Pdpn*$^{-/-}$ FRCs

plated on coverslips. Data are representative of 3 independent experiments (mean±s.d.; n>37 cells per condition). *P<0.0001 (Mann Whitney test (**a-e,g**) or one sample t-test (**f**)).

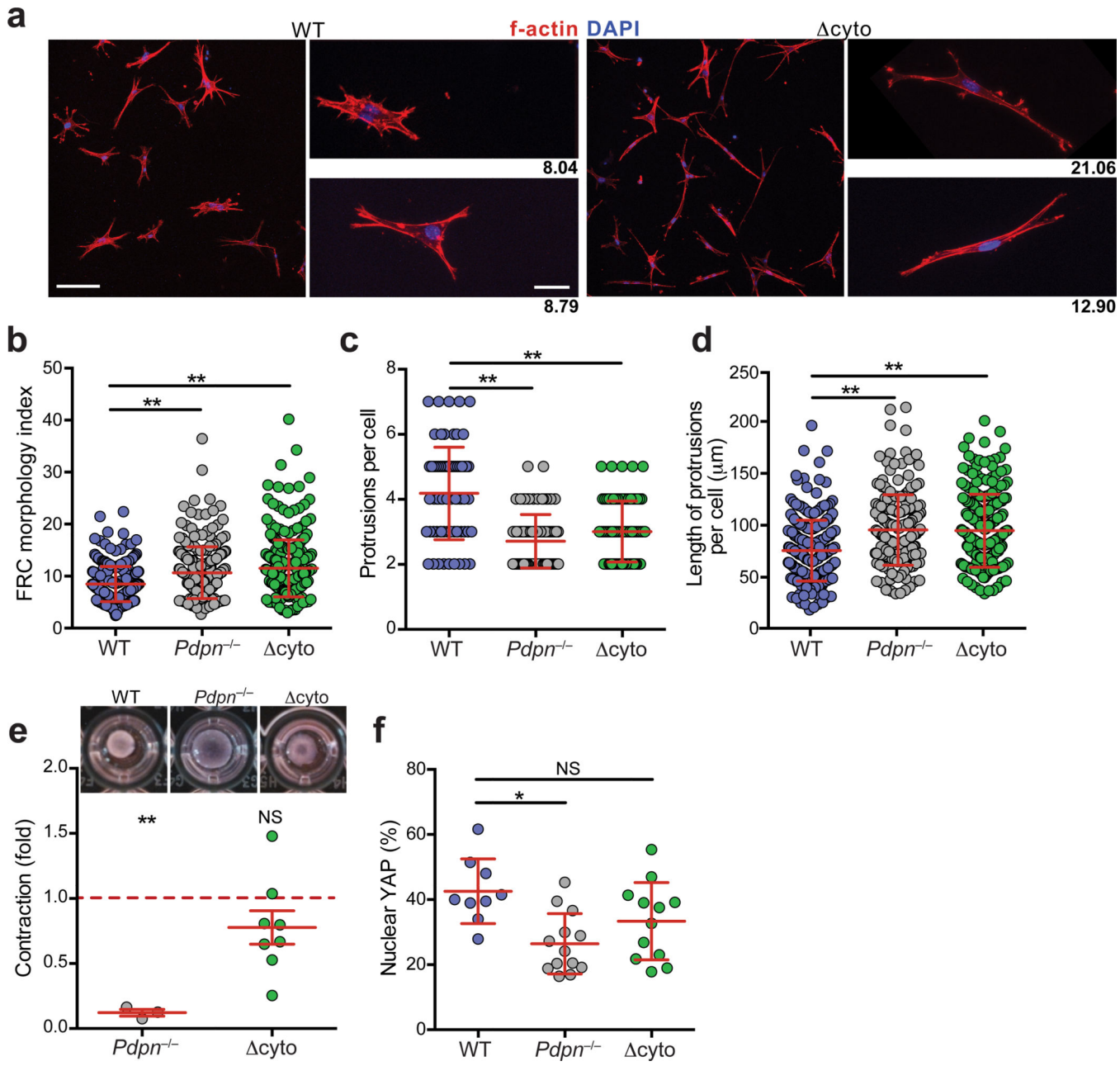

Figure 2. The PDPN cytoplasmic tail controls elongation but is dispensable for contraction

(**a**) Confocal images of wild-type and Δcyto FRCs seeded into 3D gels. Scale bar, 100 μm in low magnification images (left) and 20 μm in high magnification images (right). Numbers indicate the morphology index value for that cell. (**b**) Quantification of FRC morphology index. (**c,d**) Graphs depicting the number of protrusions per cell (**c**) and the lengths of individual protrusions (**d**) for the FRCs. Data points represent individual cells from 3 independent experiments (mean±s.d., n>50 cells per experiment). (**e**) Relative amount that *Pdpn*$^{-/-}$ and Δcyto FRCs contracted collagen gels relative to wild-type FRCs. Data are representative of 3–8 independent experiments (mean±s.d.). (**f**) Graph indicating percentage of active nuclear YAP in FRCs. Data are representative of 2 independent experiments (n>9

cells per experiment). n.s., not significant; *P<0.01; **P<0.0001 (Mann Whitney test (**a-d,f**) or one sample t-test (**e**)).

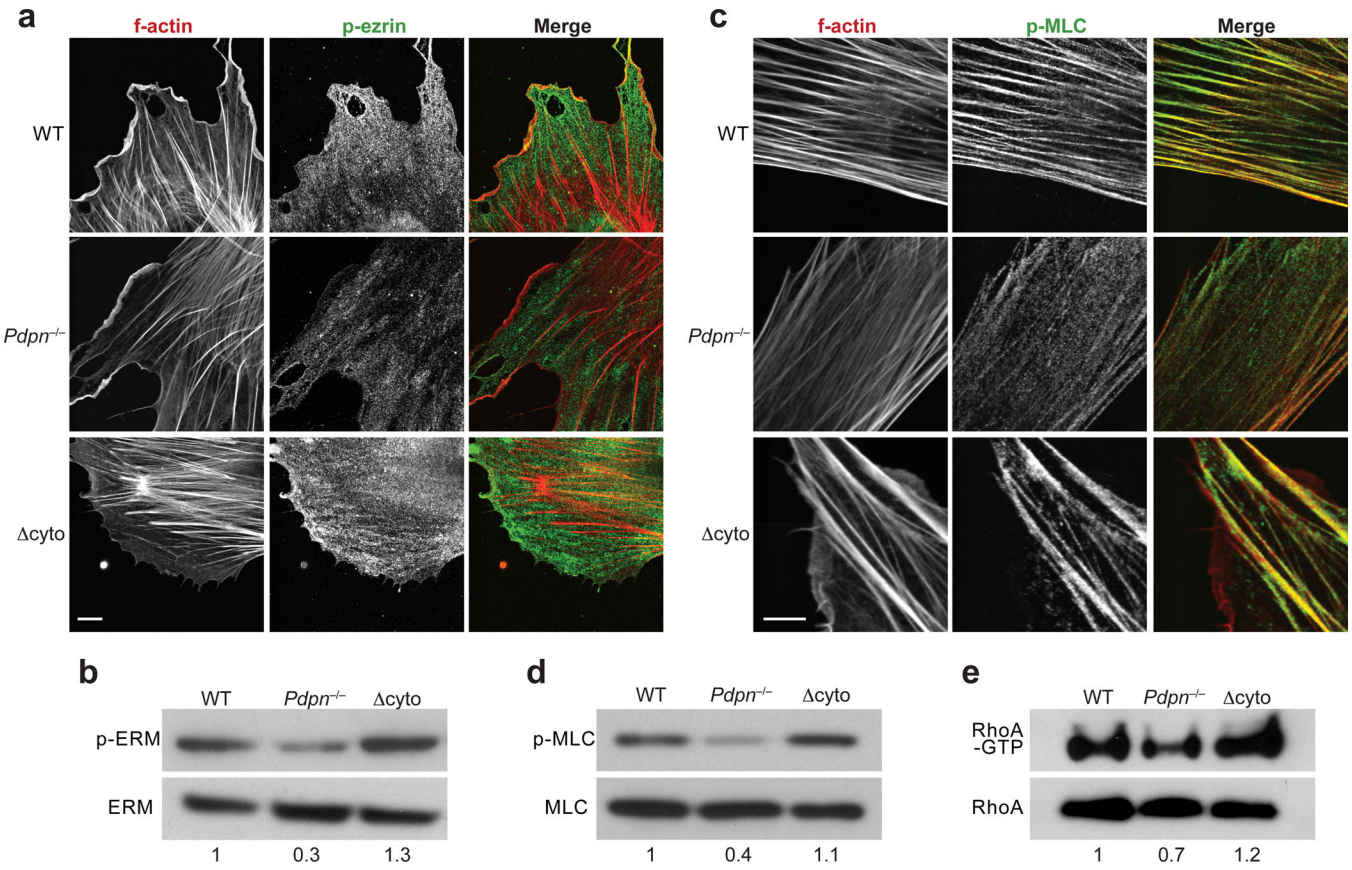

Figure 3. PDPN signals through ERM and MLC to control contraction

(**a**) Representative images depicted p-ezrin staining in wild-type, *Pdpn*$^{-/-}$, and Δcyto FRCs. Scale bar, 10 μm. (**b**) Representative immunoblot of the abundance of total and activated ERM proteins in FRCs. (**c**) Representative images of p-MLC staining in wild-type, *Pdpn*$^{-/-}$, and Δcyto FRCs. Scale bar, 10 μm. (**d**) Immunoblot of p-MLC levels in these FRCs. (**e**) Immunoblots of total and active RhoA in wild-type, *Pdpn*$^{-/-}$, and Δcyto FRCs. Numbers indicate relative band densities. Data are representative of 3–5 independent experiments.

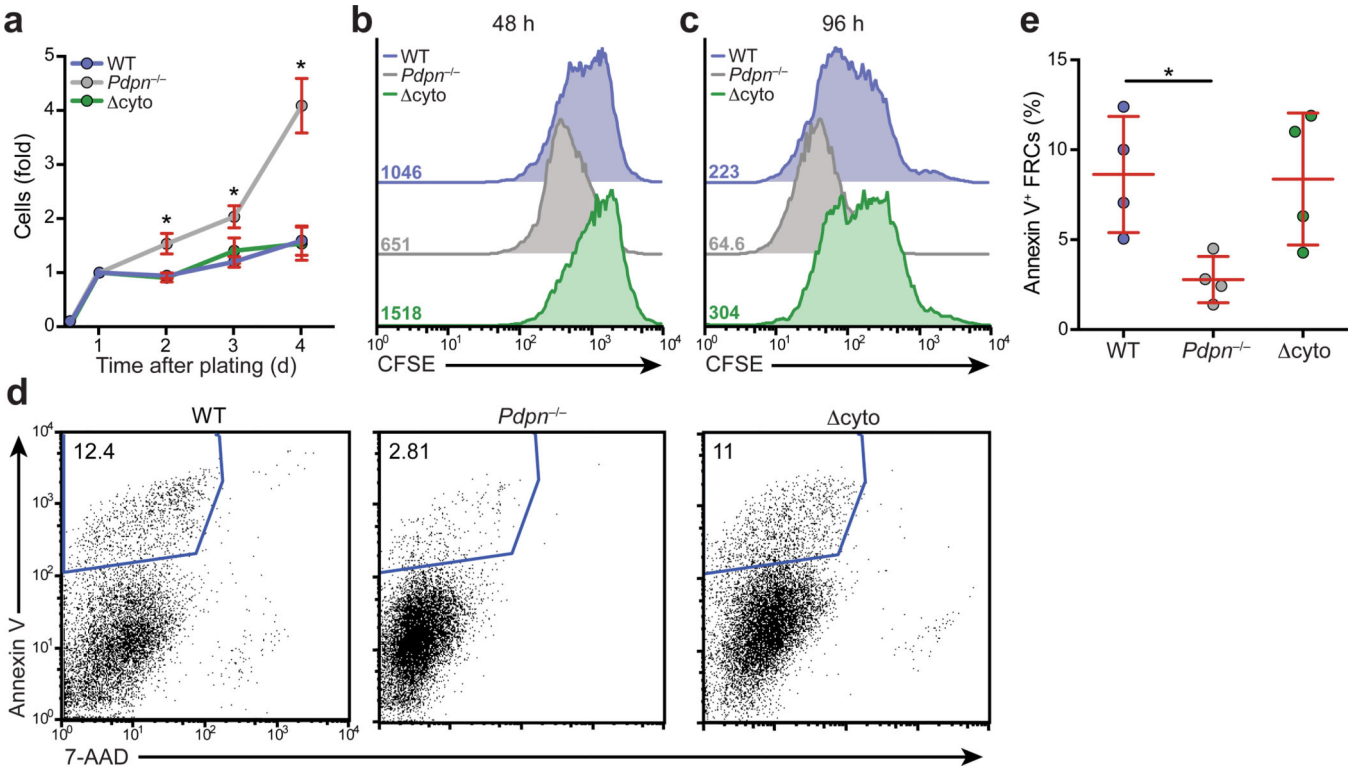

Figure 4. PDPN maintains normal FRC proliferation and survival

(**a**) Graph indicating the relative number of cells present over 4 days of culture as measured by ATP content. Data are representative of 3 independent experiments (mean±s.d., 3 wells per experiment). (**b,c**) Representative histograms indicating CFSE content in wild-type, *Pdpn*$^{-/-}$, and Δcyto FRCs after 48 (**b**) or 96 (**c**) days of culture. Numbers indicate the MFI for each condition. (**d**) Representative flow cytometry plots of Annexin V and 7-AAD staining of FRCs. Numbers indicate percentage of Annexin V^{+} cells. (**e**) Quantification of Annexin V^{+} FRCs from 4 independent experiments. *p<0.05 (Student's t-test (**a**) or Mann Whitney test (**e**)).

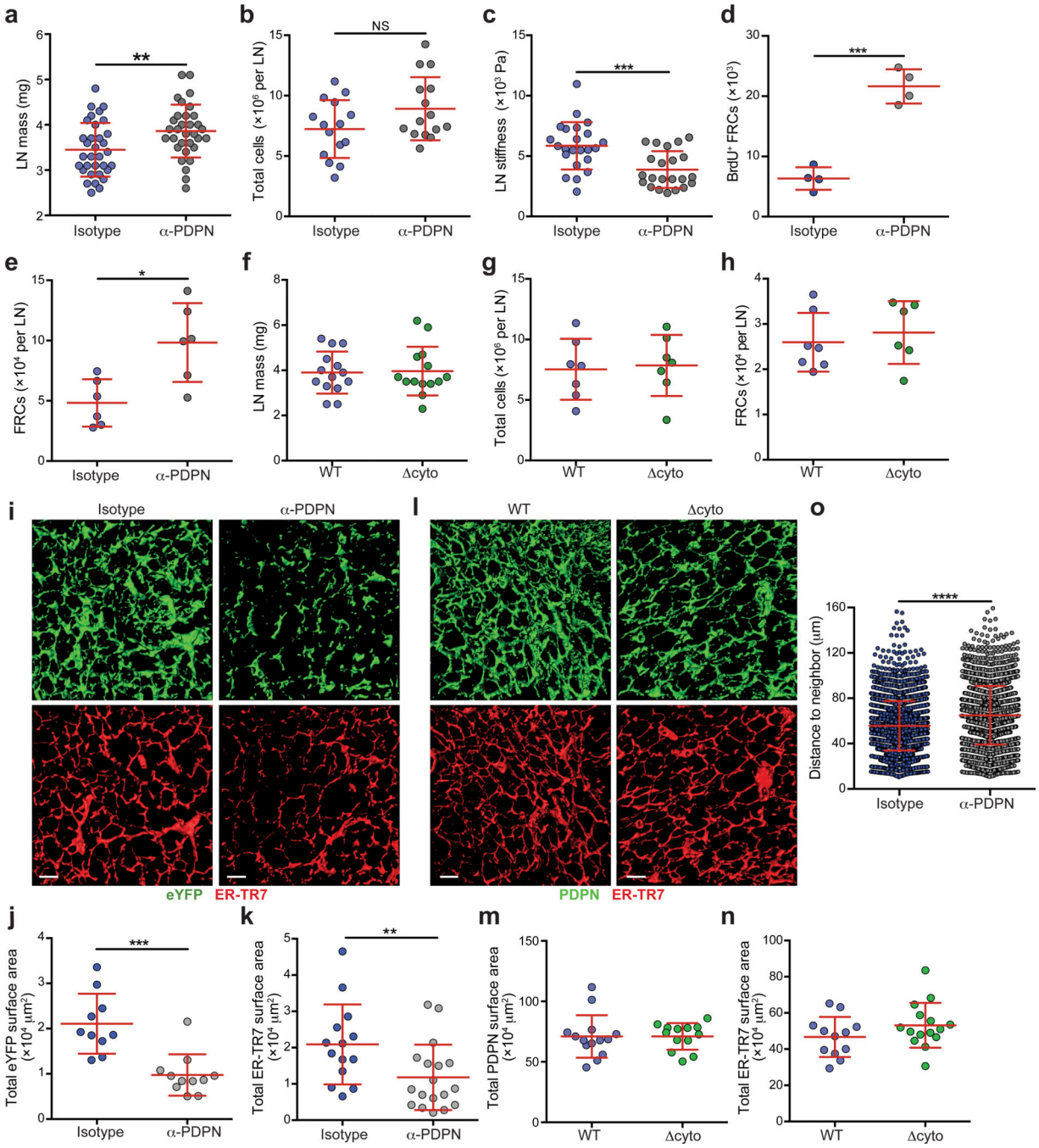

Figure 5. *In vivo* blockade of PDPN results in enlarged LNs, FRC proliferation, and a reorganization of the FRC network

(**a**) Graph indicating LN mass from mice 48 h after i.v. injection of an isotype or PDPN-specific antibody. (**b**) Total LN cellularity from isotype- or anti-PDPN-treated mice. Data represent 4 independent experiments (mean±s.d.; n>3 mice/group per experiment). (**c**) Stiffness of LNs from mice treated with isotype or anti-PDPN antibody for 48 h. Data represent 3 independent experiments (mean±s.d.; n>3 mice/group per experiment). (**d**) Graph indicating the number of $BrdU^+$ FRCs in LNs from mice treated with an isotype

control or anti-PDPN antibody. Data are representative of 3 independent experiments (mean ±s.d.; n=4 mice/group). (**e**) Total numbers of FRCs ($PI^{-}CD45^{-}CD31^{-}PDPN^{+}$ cells) in LNs from mice treated with the isotype or PDPN-specific antibody. Data are representative of 3 independent experiments (mean±s.d., n=3–4 mice per experiment). (**f**) Masses of LNs from wild-type or Δcyto mice. (**g,h**) Total cellularity (**g**) and FRC numbers (**h**) in LNs from wild-type and Δcyto mice. Data are representative of 3 independent experiments (mean±s.d., n=6–7 mice from 2–3 experiments). (**i**) Confocal z-stacks were analyzed in 3D in Imaris, and isosurfaces were generated. Representative images of the FRC network in isotype- and anti-PDPN-treated mice. Scale bar represents 20 μm. (**j,k**) The total surface area covered by the eYFP (**j**) and ER-TR7 (**k**) signals. Data are representative of 3 independent experiments (mean±s.d., n>8 fields from 4 mice per experiment). (**l**) Representative images of the FRC network in wild-type and Δcyto mice. Scale bar represents 20 μm. (**m,n**) The total surface area covered by the PDPN (**m**) and ER-TR7 (**n**) signals. Data are representative of 3 independent experiments (mean±s.d., n>8 fields from 4 mice per experiment). (**o**) The distance between the nuclei of neighboring FRCs in LN from isotype- or anti-PDPN-treated mice. Data are representative of 2 independent experiments (n>2,600 nuclei from >8 fields from 2–3 mice per experiment). n.s., not significant; **P*<0.05; ***P*<0.01; ****P*<0.001 ****P*<0.0001 (Mann Whitney test).

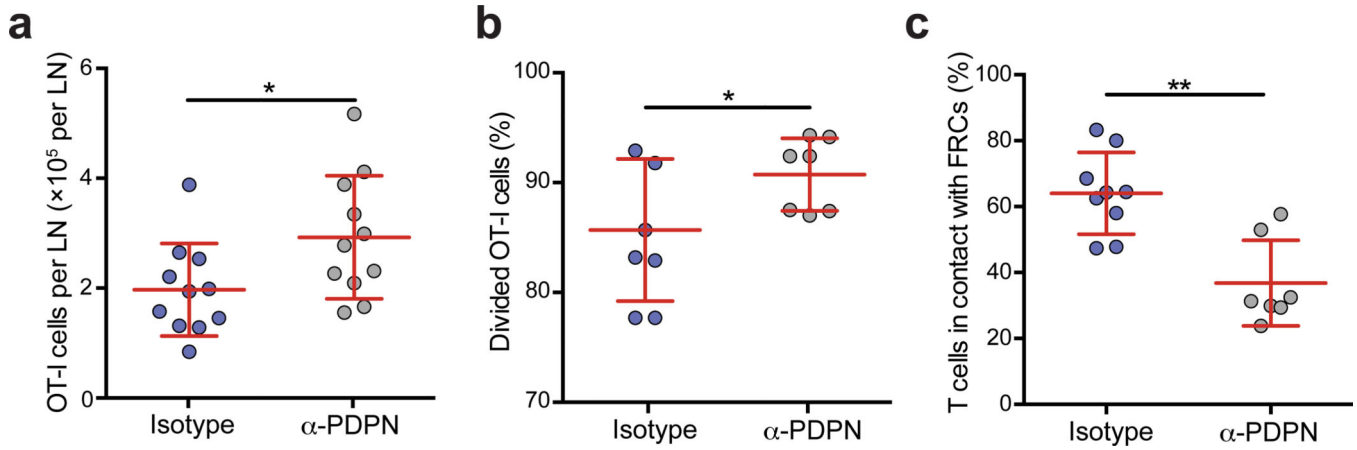

Figure 6. PDPN is required to control lymph node swelling and T cell proliferation following immunization

Mice were injected with the PDPN-specific antibody and then received OT-I T cells, LPS, and OVA 48 h later. (**a**) Number of transferred OT-I T cells in isotype- or anti-PDPN-treated mice 96 h after immunization. (**b**) The percentage of OT-I cells that divided at least once 48 h after immunization. Data are representative of 4 independent experiments (mean ±s.d. n=4 mice per group per experiment). (**c**) The percentage of T cells in contact with the FRC network in LN treated with the isotype control or PDPN-specific antibody. Data are representative of 2 independent experiments (n=2–3 fields of view from 3 mice per group). *p<0.05; **p<0.01; (Mann Whitney test).

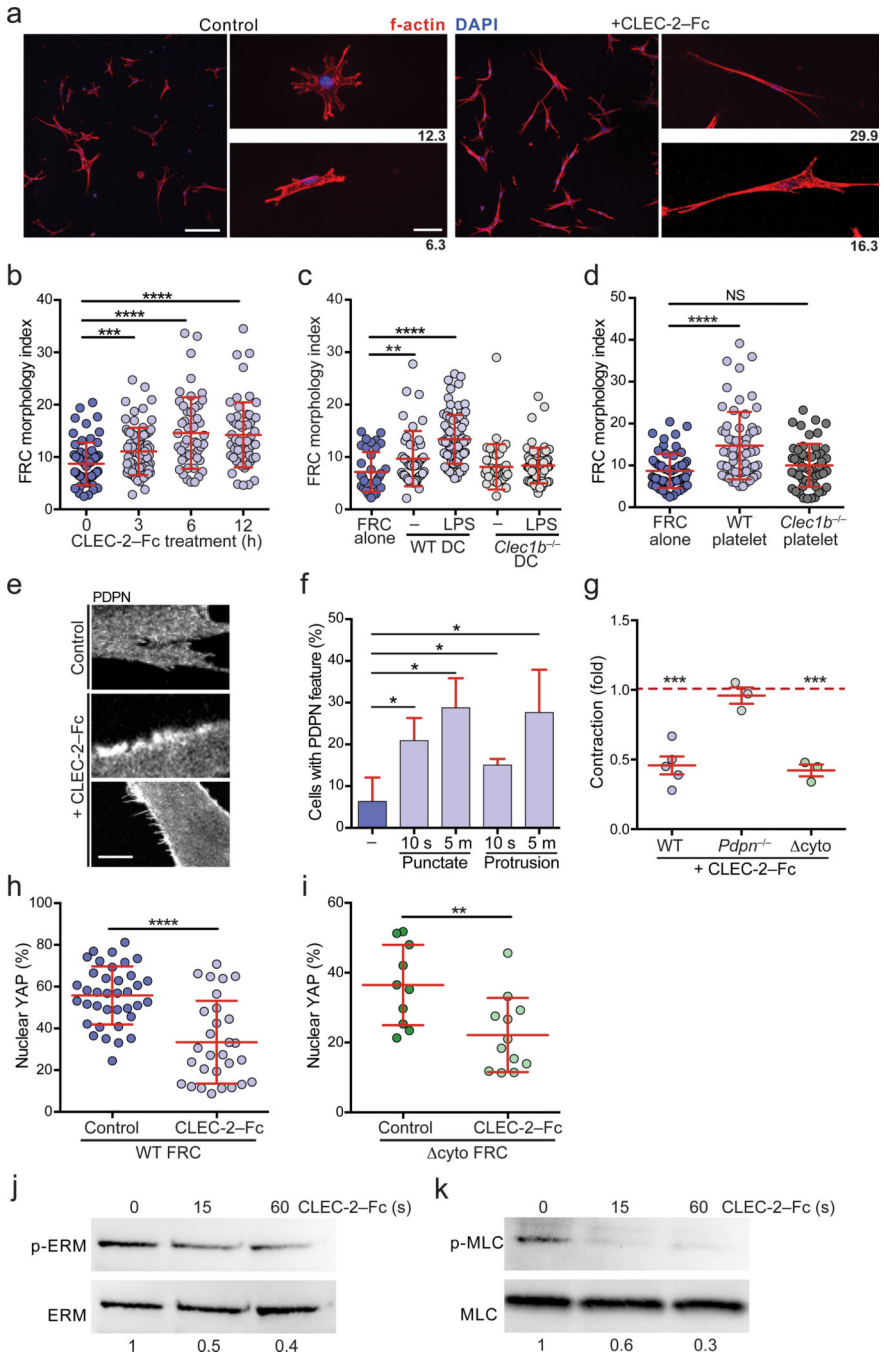

Figure 7. CLEC-2 engagement of PDPN phenocopies genetic deletion of PDPN

(**a**) Confocal images of control- and CLEC-2-Fc-treated wild-type FRCs. Scale bar indicates 100 μm in low magnification images (left) and 20 μm in high magnification images (right). (**b**) The morphology index for wild-type FRCs treated with CLEC-2-Fc for the indicated times. (**c**) Morphology index of FRCs co-cultured with wild-type or *Clec1b*$^{-/-}$ BMDCs that were either untreated or stimulated overnight with LPS. (**d**) Morphology index of FRCs co-cultured with wild-type or *Clec1b*$^{-/-}$ platelets. Data represent 3 independent experiments (mean±s.d.; n>60 cells from 5 mice for each condition). (**e**) Images of PDPN staining in

control- or CLEC-2-Fc-treated wild-type FRCs. Middle, example of PDPN clustering; Bottom, example of FRC-rich protrusions. Scale bar indicates 5 μm. (**f**) Quantification of the percentage of FRCs exhibiting PDPN clustering or protrusions in response to CLEC-2-Fc treatment. (**g**) Relative amount that CLEC-2-Fc-treated wild-type, *Pdpn*$^{-/-}$, and Δcyto FRCs contracted collagen gels, relative to control-treated wild-type, *Pdpn*$^{-/-}$, and Δcyto FRCs, respectively. Data represent 3–5 independent experiments (mean±s.d., 3 wells per experiment). (**h,i**) Percentage of nuclear-localized YAP in control- or CLEC-2-Fc-treated in FRCs from wild-type (**h**) or Δcyto (**i**) mice after 24 h. Data are representative of 3 independent experiments (n>10 cells per experiment). (**j,k**) Representative immunoblots of p-ERM (**j**) and p-MLC (**k**) in wild-type FRCs treated with CLEC-2-Fc for the indicated times. Numbers indicate relative band densities. n.s., not significant; **P*<0.05; ***P*<0.01; ****P*<0.001; *****P*<0.0001 (Mann Whitney test (**b-d,f,h,i**) or one sample t-test (**g**)).

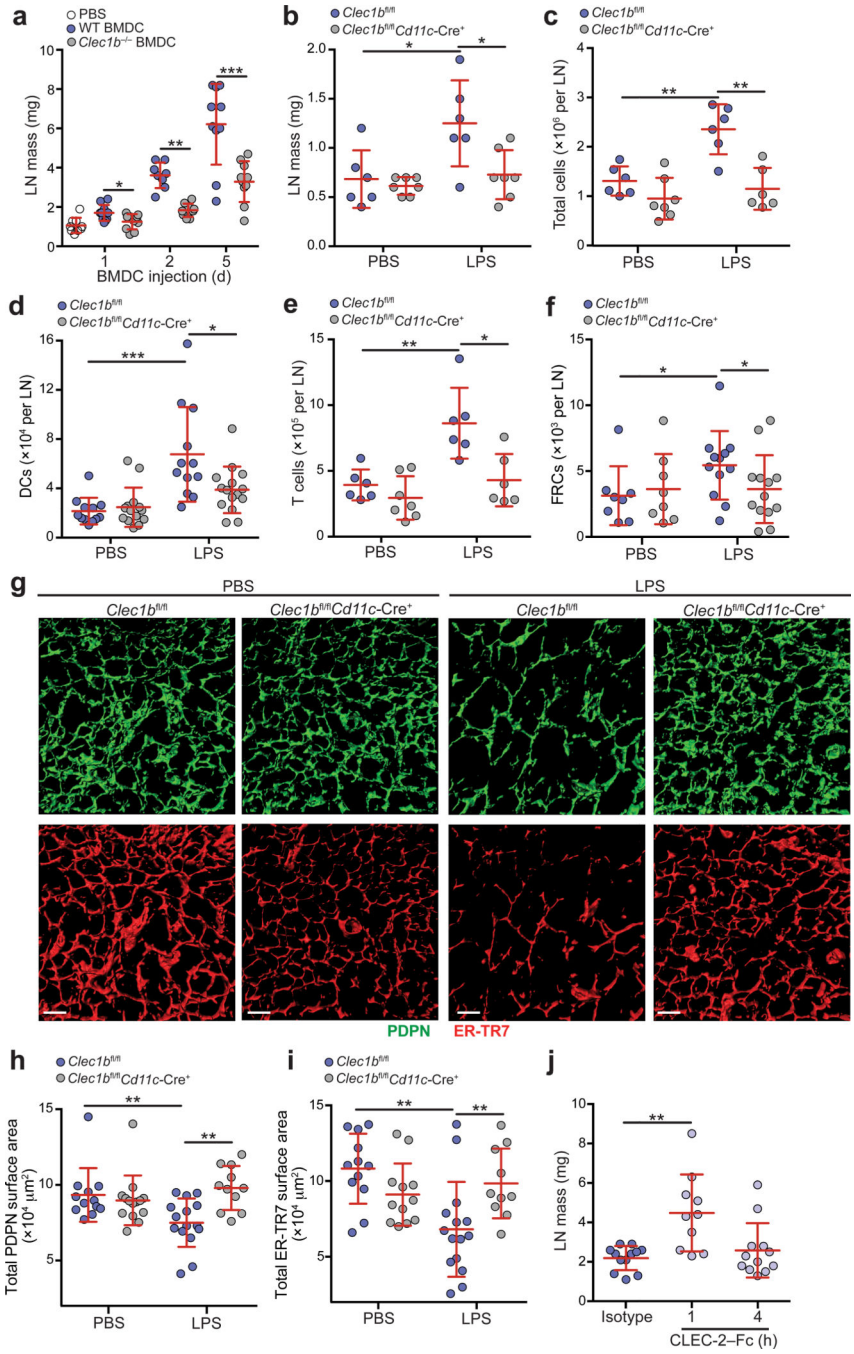

Figure 8. CLEC-2 signals from migratory DCs are required for expansion of LNs and the FRC network in response to immunization

(**a**) Mice were injected with wild-type or *Clec1b*$^{-/-}$ BMDCs in the footpad, and the draining LNs were weighed 1, 2, and 5 days later. (**b-f**) *Clec1b*$^{fl/fl}$ and *Clec1b*$^{fl/fl}$*Cd11c*–Cre^{+} mice were injected into the footpad with PBS or 8 μg of LPS and popliteal LNs were collected 24 h later. Graphs depict LN mass (**b**), total cellularity (**c**), and number of DCs (**d**), T cells (**e**), and FRCs (**f**) present in the LNs. Data are representative of 4 independent experiments (mean±s.d. n≥3 mice per experiment). (**g**) Representative images of the FRC network in

LNs from *Clec1b*$^{fl/fl}$ and *Clec1b*$^{fl/fl}$*Cd11c*–Cre^{+} mice. Confocal z-stacks were imaged in 3D and isosurfaces were generated. (**h,i**) Quantification of the total surface area covered by the PDPN (**h**) and ER-TR7 (**i**) stains in **g**. Data are representative of 2 independent experiments (mean±s.d. n=8–9 fields of view from LNs of 3–4 mice per experiment). (**j**) Masses of LNs from wild-type mice treated i.v. with an isotype control or CLEC-2-Fc for 1 or 4 h. Data are representative of two independent experiments (n=3 mice per group per experiment). **P*<0.05; ***P*<0.01; *** *P*<0.0001 (Mann Whitney test).